Published by SET Publisher

Journal of Basic & Applied Sciences

ISSN (online): 1927-5129

Modeling and Simulation in Cancer Nanomedicine

Keka Talukdar*

Department of Physics, Nadiha High School, Durgapur-713211, West Bengal, India

Article Info:

Keywords:
Modeling and Simulation,
Cancer,
Ion channel,
Nanomedicine,
molecular dynamics.

Timeline:
Received: April 04, 2021
Accepted: June 04, 2021
Published: June 10, 2021

Citation: Talukdar K. Modeling and Simulation in Cancer Nanomedicine. J Basic Appl Sci 2021; 17: 53-63.

DOI: https://doi.org/10.29169/1927-5129.2021.17.06

Abstract:

There is a certain function of ion channels in cancer cell progression and proliferation. The mutation of ion channels is proved to have a clear influence on the same. The progress of nanomedicine research needs the proper concept of the exact role of ion channels in cancer and the cause of the disease. In this work, an ion channel protein residing in our stomach with PDB id 3ux4 is analyzed to get an idea about its structure-function relationship. The disordered region and mutation sensitivity of the channel causing cancer are analyzed in different ways. Eight disordered regions of the protein are found in the study. The pocket in the active site is found along with the position of the miss-sense mutation. The maximum mutation region is also found for a sample disordered region. The engineered ion channel is simulated in the environment of water and ions. The potential energy of the water-ion model of the protein calculated by molecular dynamics simulation is 20,412 kcal/mol after simulating the system for 1,00000 steps.

*Corresponding Author
E-mail: keka.talukdar@yahoo.co.in

INTRODUCTION

It was always an effort to treat fatal diseases like cancer efficiently by targeting specific cancerous cells without harming the healthy ones. The highly target-specific drug delivery can only be achieved by nanomedicine (NM). NM works by binding its surface with different kinds of ligands such as antigens, antibodies, enzymes, etc. where NM is encapsulated within a drug delivery carrier. This is called active targeting and this method is the most popular compared to passive targeting [1]. For different fatal diseases, pre-clinical trials are being envisaged with liposomes [2-4], dendrimers [5, 6], polymeric nanoparticles (NPs) [7, 8], magnetic NPs [9, 10], carbon nanotubes (CNTs) [11, 12], etc. Some NPs are already in use for clinical trials, though they lack some vivid toxicological knowledge. More than 100 cancer nanodrugs got FDA approval, but expected success is yet to come. That means these drugs need further investigation before trial.

At this stage, modeling and simulation play a vital role in various aspects of cancer-related treatment. Such studies include the mathematical modeling of the accumulation of NPs in tumour cells [13], modeling the process of glioblastoma growth in the avascular stage [14], modeling of the NP intake of the tumorous cells, and the dependence of efficacy of nano-drug delivery on the tumour microenvironment [15]. The modeling and simulation studies on the various factors affecting the nano-drug delivery are explicitly done by Dogra *et al*. and Sahai *et al*. recently in two independent studies [16, 17]. Physiologically based pharmacokinetic (PBPK) modeling by Cheng *et al*. [18] explored the dependence of various factors on NM delivery to the timorous tissues by modeling and simulation. The early stage of the growth of brain tumours is mainly discussed in their study.

Apart from the above studies, researches on the role of ion channels in cancer have opened several possibilities for cancer detection and therapy in the medical field. Though cancer is not marked as a channelopathy [19], the role of ion channels on cancer cell migration and proliferation is gaining attention rapidly. Finding the proper channel expression and the modifying factors for the cancer-specific channels is important in understanding the progression of the disease. Not only that, the proper knowledge may help its therapeutic cure [20]. The behavior of ion channels in cancerous cells and immune cells is different in respect of Ca^{2+} signalling. The alteration of calcium ion efflux is related to the activation or suppression of immune cells for the progression of cancer. The intracellular Ca^{2+} homeostasis is regulated by the proper functioning of mitochondrial ion channels [21]. The dependence of cancer cell progression and migration on ion channels is discussed by Litan and Langhans [22].

The ion channels show abnormal or different behavior for cancer cell lines compared to the channels found in normal cells. Now scientists are believing that there is a clear role of ion channels in cancer cell migration and proliferation. Ca^{2+} permeable channels, K^{+} and Na^{+} channels are responsible for carcinomatous cell growth [23]. Ion channels malfunctioning can hinder normal physiological processes. The normal working of channels is necessary to maintain essential processes like cell proliferation, migration, and apoptosis. Mainly the ion channels in mitochondria play a significant part in cell birth to apoptosis, their modification may be a vital process of death of cancer cells. Managing the channel function can manage tumour growth. Computational modeling and simulation of ion channels, their signalling mechanism are also reported in many pieces of literature. Some of the recent findings are remarkable. Storm *et al*. [24] simulated a protein-lipid complex HAMLET to investigate the influence of ion fluxes on the tumour cell death process and therapeutic cure for cell death. They also suggested an immune response of the healthy tissues outside the carcinogenic cells triggered by HAMLET. Modeling and simulation of hERG and hEAG potassium channels found the role of clofilium as a channel blocker to resist cancer progression [25]. Not only the biochemical signalling mechanism based on a single cell pattern is important, but the signalling pathway for electrical coupling between cells is described by Cervera *et al*. [26].

To understand the role of the ion channel in cancer, in the present study the ion channel protein with PDB id 3UX4 is simulated in different conditions to understand its structure-function relationship. The bacteria Helicobacter pylori reside in the stomach and it survives in the acidic environment. The ion channel protein with PDB entry 3UX4 is responsible for helping urea to pass through the open channel pore and neutralizes acid in the stomach and the bacteria gets the opportunity to survive. The present work is a computation analysis of the ion channel protein with PDB id 3UX4, malfunctioning or mutation of which may cause cancer in humans. To get a vivid knowledge of

its functioning, the ordered and disordered regions of the ion channel are predicted, the amino acid mutation is observed, and ligand binding sites are found. The dipole and quadrupole moments are also calculated. Lastly, Molecular dynamics (MD) simulation is performed for the ion-water model of the protein that can give deeper insight into the interaction and behavior of the protein in the body environment.

METHODS AND MODELING

The protein structure is generated by Protein Homology/analogy Recognition Engine V 2.0, Phyre2 [27] from the fasta file. The software compares the given protein structure to almost 1,77655 (as of 11th May 2021 in rcsb.org) known structures. Then the structure is aligned to the pattern generated by evolutionary variation of known sequences. This is called Template-based homology modelling which is followed by Phyre2. Unlike other structure-predicting engines, Phyre2 can focus on the main sequence to match with other known structures. On submitting the FASTA sequence to the software, the protein structure in the template can be generated. The main active template structure of template name c3ux4C of 1-201 residues are aligned with 99% confidence. Information on this template can be obtained by running the investigator once again. The algorithm for the structure prediction is as follows [27].

1. In the first stage, HHbuilts generate HMM(Hidden Markov Model) with the help of PSI-Pred. At this stage, the secondary structure is also found

2. HHSearch compares the HMM with all known structures. Alignment is done and the backbone only crude model is generated.

3. Loop modeling is done to achieve the correct sequence after addition and deletion

4. In the last stage, the final model is obtained by adding side-chain fragments

Ligand binding site prediction is done by the 3D ligand Site-Ligand Binding Site Prediction Server [28]. The ion channel pore is generated using CHarmm7 potential in Charmm-gui software. A detail of the protein structure is obtained from Phyre2.

The Ramachandran Plot [29] is the plot for a residue for φ and ψ angles. After plotting, the residue is colored according to favorable (green), allowed (blue), and disallowed (red). The rotamers are nothing but the region in the residue which was not modeled properly. The main problem is the alignment of the region.

The alignment confidence of a residue is calculated by HHsearch available in Phyre2. Pocket detection is done by fpocket [30]. The miss-sense mutation in a template is found by SuSPect [31] by assigning scores to the mutation so that it can be associated with disease or not.

RESULTS AND DISCUSSION

The Structure of the Ion Channel

The urea ion channel of Helicobacter pylori has a huge role in stomach cancer [32] in human. Figures **1** and **2** show the protein structure and engineered pore modeled from the PDB entry 3UX4 respectively. The protein structure contains transport protein, lyase, signalling protein, sugar-binding protein, Cysteine proteinases, transferase, hydrolase, de novo protein, prealbumin like protein, plectin, some structural proteins, retinol-binding protein, metal transport domain, immunity protein, lipid-binding domain, hydrolase inhibitor, membrane protein, and toxin. The information is extracted from Phyre2 search. The secondary structure contains 71% alpha-helix, 54% TM

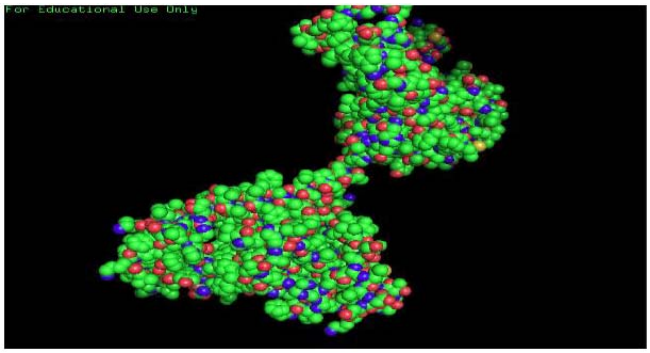

Figure 1: Protein structure of pdb entry 3UX4.

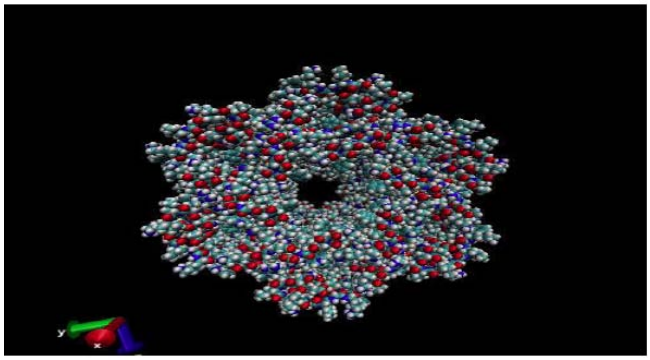

Figure 2: Engineered ion channel pore.

helix, and 20% disordered region. The structure contains 376 aligned regions.

The protein with identifier c3ux4C is a transport protein that is an acid-activated urea channel from the human gastric pathogen2 helicobacter pylori. The template structure contains 180 aligned residues. Disorder in this sequence is important to know as it is the most flexible regions which may prevent normal physiological function. Figures **3-6** are the analysis result of template c3ux4C. Disordered regions, rotamer positions, alignment reliability, and Ramachandran plot are depicted in these figures respectively. The disordered regions show the regions where the structure is flexible and highly dynamic. This structure shows moderately high disordered regions in some places. Disorder in the urea ion channel in H. Pylori was experimentally proved by Strugatsky *et al*. [33]. Figure **7** shows the score of disorder tendency with respect to residue number. Score 1 means completely disordered structure where 0 means ordered. High score to low score gives high to moderate disordered regions. All the results are obtained from Phyre2 online software.

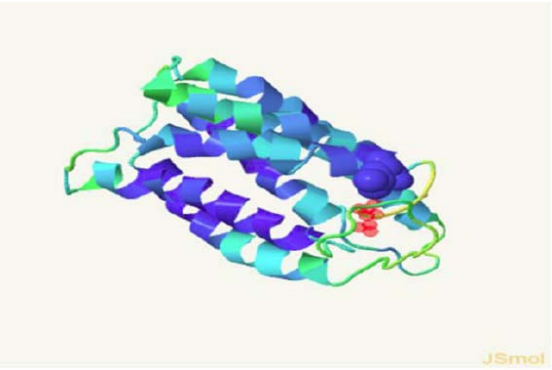

Figure 3: Disordered region of the transport protein template region c3ux4C. The most disordered region is colored in red. Green and light blue represent moderately disordered region. Disordered regions are mobile in nature unlike ordered ones and play important role to preventsuccessful crystallization.

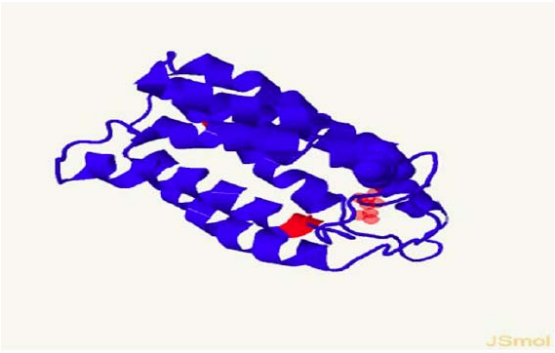

Figure 4: Position of rotamers in template information of c3ux4C. Red region is not modelled ideally and may produce unreliability in backbone alignment.

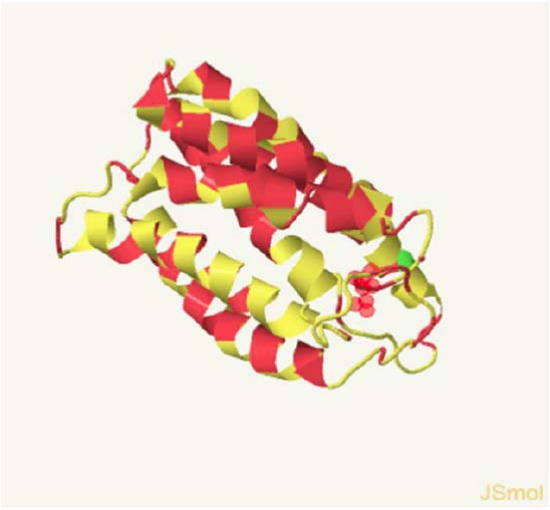

Figure 5: Pairwise template alignment reliability The reliability is calculated in the Forward- Backward algorithm. Red color defines good alignment and blue color (absent here) represents bad alignment probability. The yellow color is.of moderately high alignment reliability.

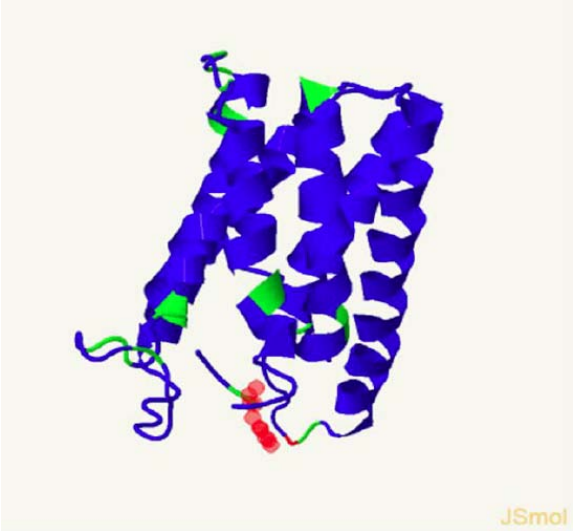

Figure 6: Ramachandran plot of the template id c3ux4C. It indicates the torsion angles φ and ψ. High structure reliability can be obtained in the blue color regions while the red color means less reliable. Green is moderately reliable portion.

Disordered regions are mostly obtained for the following residues. The amino acid sequence for this template is ARNDCQEGHILKMFPSTWYV. The disordered regions are observed for residue names, MET1, TYR94, TRP112, SER114, TRP152, TRP189, MET202, TYR295, etc.

The alignment reliability of the template is high to moderately high. The pockets in the active site are

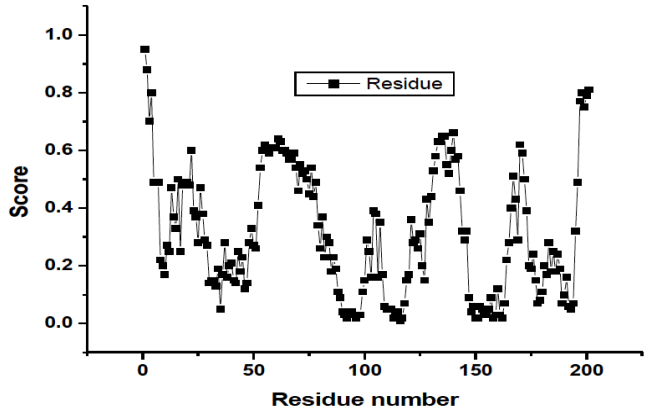

Figure 7: Disorder score with respect to residue number for the ion channel.

shown in Figure **8**. It is the indicator of the site of binding with chemical species and is the most important part of the urea channel. Figure **9** reveals the position of the missense mutation. Mutation of genes and missense mutation was observed in animals by Suzuki *et al*. [34] experimentally that confirms the prediction of mutation sensitivity in the channel. Mutation has huge importance in computational biology as this means, at this position only a single nucleotide changes the structure into another nucleic acid. In the template c3ux4C, the sequence profile and maximum mutation are given in Figure **10** for a definite residue MET1. The red color region is an indication of maximum mutation position. The mutation is responsible for functional changes in any protein including ion channels.

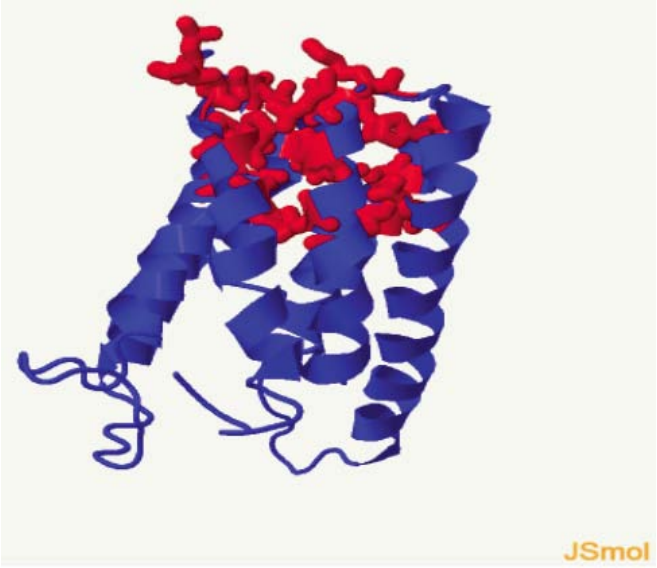

Figure 8: Pockets present in the template with id c3ux4C. The position of the large pocket indicates the location of the active sight. The active pocket is shown in red color in wire-frame model.

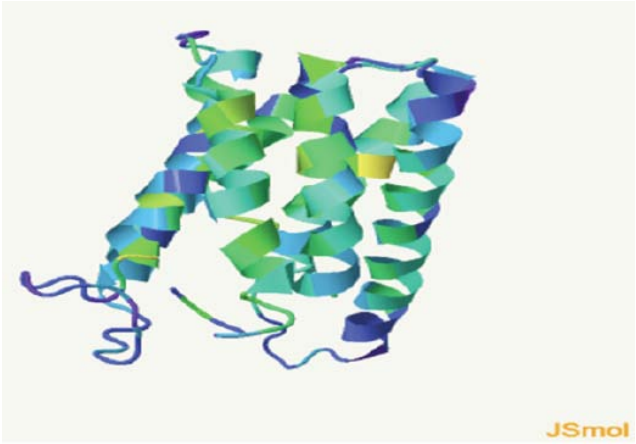

Figure 9: Position of the probable missense mutation. Red color means large probability. Yellow and green color indicates moderately high probability of missense mutation at these sites.

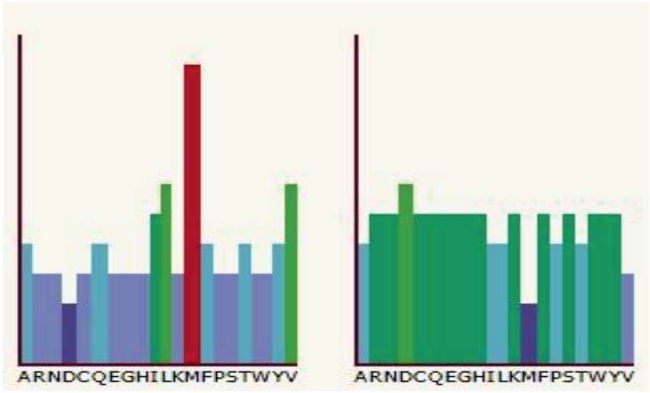

Figure 10: Residue MET1 sequence profile (left) and the mutation (Right). Red color shows the maximum disordered region in the left.

The mutation sensitivity is checked thrice to get the variance of results by ANOVA test. The results are given in Table **1**.

Table 1: The Results of One-Way ANOVA Test for the Mutation Sensitivity of the Ion Channel

Data	Mean	Variance	N
1	2.88557	2.72184	201
2	2.84577	2.60109	201
3	2.88557	2.72184	201

F=0.03958.
P= 0.9612.

As the significant level is 0.05, hence the means are not significantly different. So the little difference of results in the three trials may be due to sampling error in calculation. There is no such difference of results for multiple calculations for disorder prediction.

Now the ligand-binding sites are investigated. Figure **11** shows the ligand binding of the protein. Predicted binding sites are 404 LEU, 407 VAL, 442 SER, 489 GLY and 492 PHE. Ligand binding of the protein ion channel with PDB id 3UAX is experimentally proved by Strugatsky *et al*. [33]. The presence of metallic heterogeneous is found in the ligand-binding method. The heterogeneous are CHD, HEM, MG, FE, CLA and ZN with count 9, 10, 1, 3, 1 and 63 respectively. Ligand-binding is important as an electrical signal is produced at the site which may serve as the binding site of drugs or therapeutic agents. Perfect contact is observed for SER, then VAL has an average distance of 0.09 Å, and GLY 0.12 Å.

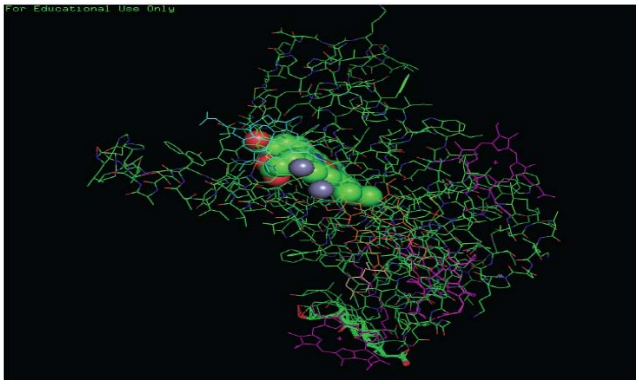

Figure 11: Ligand binding of channel protein with pdb entry 3ux4. Binding site is shown with light green and red color. Purple colored spheres represent metallic heterogens and cyan, orange, magenta colors show nonmetallic heterogens.

Dipole and Quadrupole Moments

The protein as a whole contains 4482 atoms. The dipole moment as calculated from the software abalone is 1.08187e+008 Debye where

X= -1.41797e+007 D, Y= 1.07225e+008 D, Z= 2.47786e+006 D.

Table **2** shows the quadrupole moment of the protein in different directions.

Molecular Dynamics Simulation of Ion Channel

The minimized energy of the protein structure is found as 43778.71 kcal/mol. The structure is minimized by Materials Studio 6.1 software in Forcite module by Smart minimizer.

The engineered ion channel is then simulated using MD simulation in the environment of ion and water. First, to find the pore radius and area of the protein, the protein is oriented along the z axis. Then the radius is found. The pore radius and area are plotted in Figures **12** and **13** respectively. The calculated values of pore radius and area are as follows.

Pore Minimum Radius: 21.1301669 Å, Pore Maximum Radius: 48.1975099 Å, Protein Top Area:7134.5358 unit, Protein Bot Area: 7606.4338 unit, (Pore radii are determined in -15 < Z < 15).

The next part of the calculation involves the building of a water ion system. The box is generated by Charmm potential. System size in X, Y, Z directions is as follows

X_{min}= -78 Å, X_{max}= 78 Å, Y_{min}= -81.5 Å, Y_{max}= 81.5 Å, Z_{min}= -69.5 Å, Z_{max}= 69.5 Å

The box is filled with K^+ and Cl^- with a concentration on the top and bottom of 0.15 M. Dielectric constant of protein and membrane is assumed to be 2. Cation current and anion current are assumed to be 0.196 Å2/ps and 0.203 Å2/ps respectively. Simulation of such a system gives necessary information of the nature of the interaction of the protein with body environment as the human body consists of water and ions. Figure **14** represents the ion-water system of protein. The structure is optimized using Smart Minimizer first. It is again energy minimized twice for relaxation of the structure. After the relaxation of the structure several times, the new structure looks as given in Figure **15**. Then molecular dynamics simulation is performed using Universal energy with time step 1 fs for 1,00000 steps in NVT ensemble. The nose thermostat is employed for this purpose. As in this ensemble, energy is not constant, it varies a lot and ultimately comes to an almost fixed value.

The standard deviation of data is taken after running several simulations for 30,000 steps by varying the stimulation parameters slightly. Simulation parameters

Table 2: Quadrupole Moment of the Protein with pdb id 3UX4

Direction	XY *(e+007) Buckingham	YY *(e+007) Buckingham	ZZ *(e+007) Buckingham	XZ *(e+007) Buckingham	YZ *(e+007) Buckingham	(XX-YY)/2 *(e+007) Buckingham
Quadrupole moment	-213.194	253.163	-39.968	-74.632	11.590	-233.179

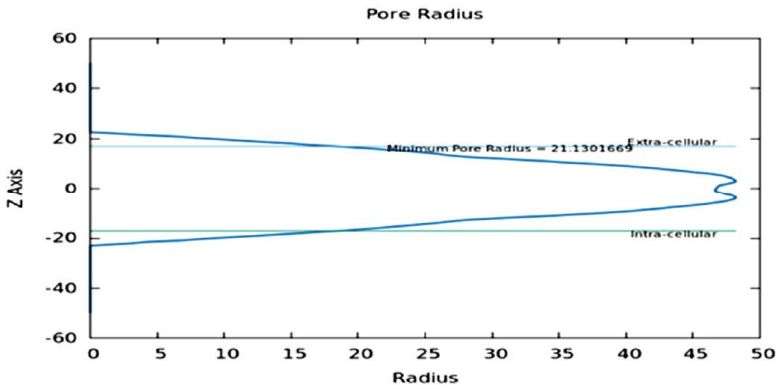

Figure 12: Pore radius of the protein with PDB ID 3UX4.

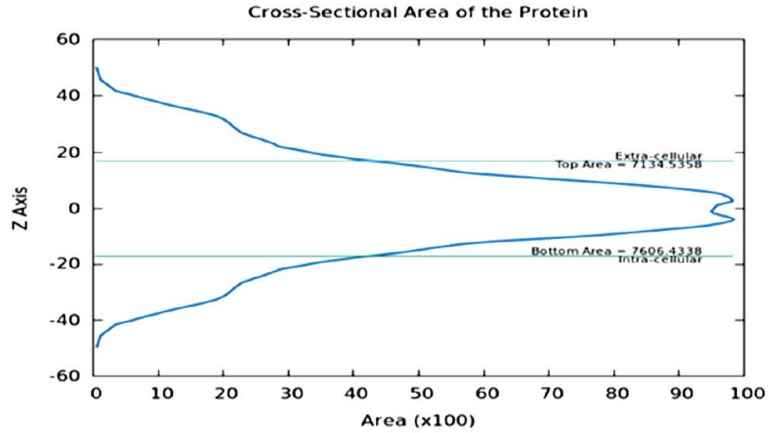

Figure 13: Cross-sectional area of the protein with pdb id 3UX4.

like temperature, time step, Coulomb cut-off distance, etc. are slightly changed and the energy curves are drawn. Standard deviations are found for 30,000 steps and statistical error bars are drawn on the average of the multiple curves. As a large variation in energy is observed in the beginning, and then slowly it comes to a much stable value, hence the data for the last 20000-30000 steps are taken for calculating standard deviation and error bars. Table **3** gives the mean, standard deviation (SD), standard error (SE), Maximum, minimum and range of data for four sets of value. Figure **16** depicts the error bars on the average potential energy curve. All the results for potential energy lie within the length of the error bars. Similarly, other errors are also within the limit as calculated for the potential energy. Figure **17** represents the error bar for the temperature. The lengths of the error bars are smaller than the lengths of the error bars for potential energy. Figure **18** represents the simulation energies for 1,00000 steps.

The simulation trajectory shows a strong hydrophobic nature of the protein. Some bonds of the protein are broken keeping the main structure intact otherwise (Figure **19**). It is also observed that water passes through the pore of the ion channel during simulation. The nature of the movement of water through the pore and that outside the pore is different. The Water inside the pore moves very slowly unlike the outside water molecules which diverge very fast from the protein. The observation is also supported by other published work [35, 36]. Simulation outcomes may help the researchers further progress in targeting ion channels for therapeutic use.

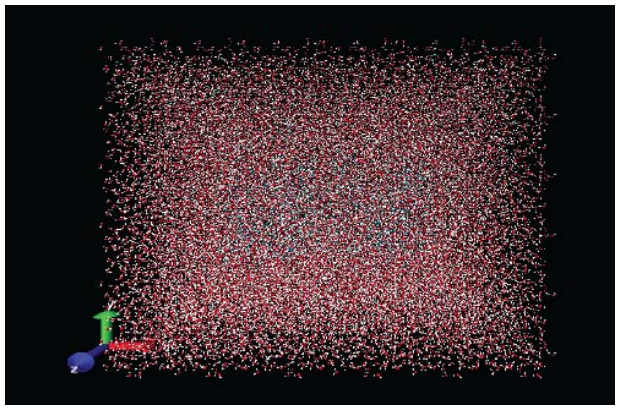

Figure 14: The water-ion model of the ion channel.

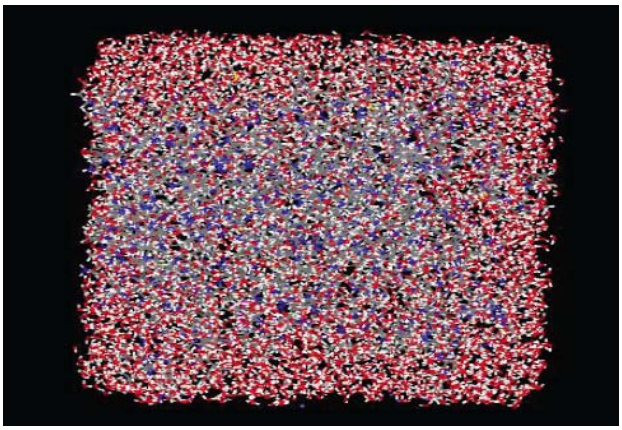

Figure 15: The water-ion model of the ion channel after relaxing the structure completely.

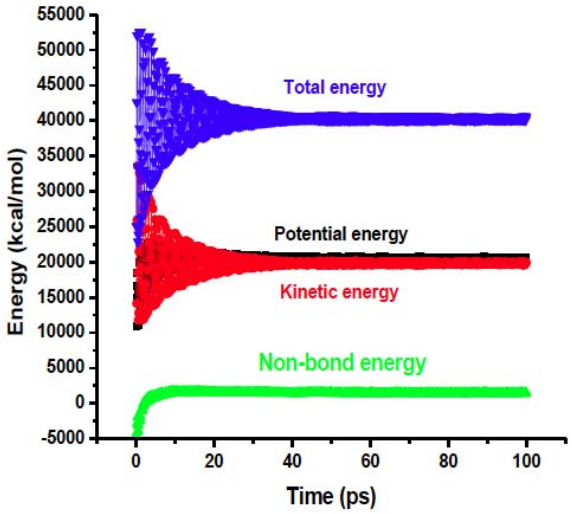

Figure 18: Energy profile of MD simulation after MD simulation.

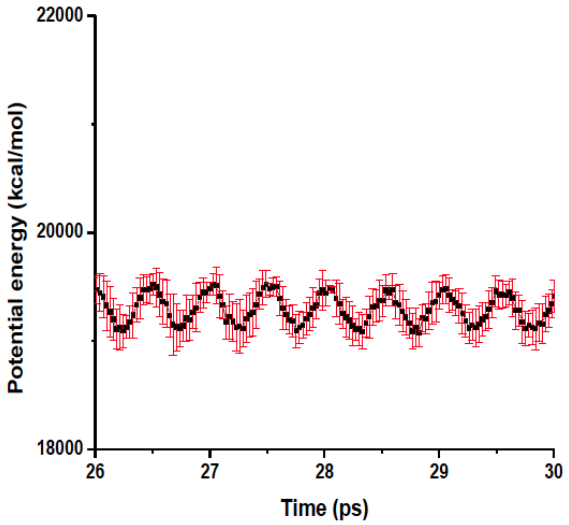

Figure 16: Statistical error bars for the calculation of potential energy of MD simulation.

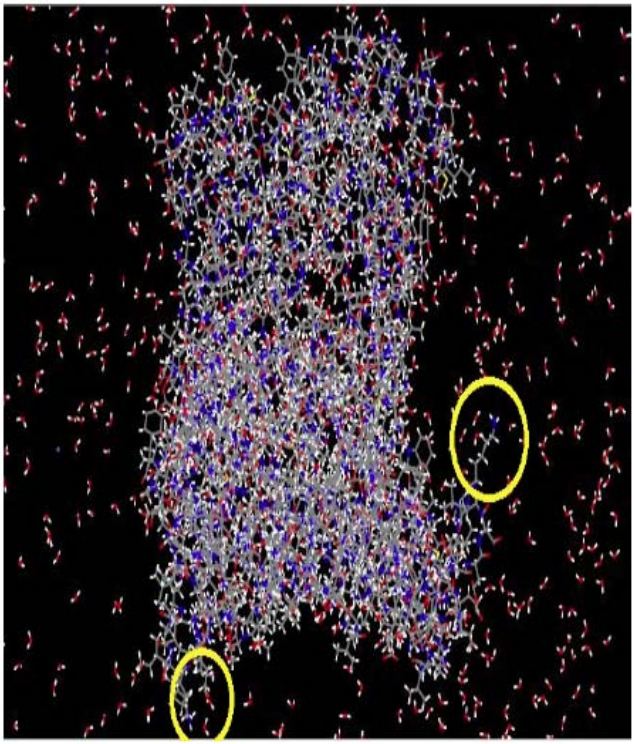

Figure 19: The water-ion model of the ion channel. The yellow circles point towards the breaking of bonds in the protein.

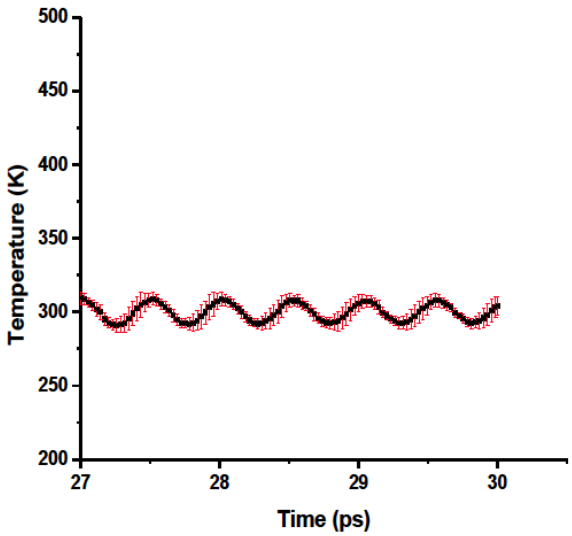

Figure 17: Statistical error bars for the calculation of temperature.

ANOVA calculation results are also shown in Table **4** for four sets of columns where the energy values are only taken for 20000-30000 steps of simulation.

the means are significantly different. This is true because for a NVT ensemble where energy does not remain constant. The ANOVA test for temperature shows some difference too, but not significant.

Table 3: SD, SE, Minimum, Maximum and Range of Data for 4 Sets of Values of Energy

Mean energy (kcal/mol)	SD	SE	Min	Max	Range
19246.35156	163.69414	81.84707	19032.07617	19374.83594	342.75861
19277.98438	155.63007	77.81503	19069.7207	19422.07813	352.35727
19342.75	127.72398	63.86199	19190.95508	19488.85352	297.89877
19410.82422	149.01761	74.5088	19259.26953	19584.42383	325.15549

Table 4: ANOVA Test Results for Four Sets of Values of Potential Energy

Data set	Mean	Variance	Number
A	19303.27602	26164.35053	136
B	19305.69128	40955.49287	136
C	19134.47589	26670.35638	136
D	19420.71917	13637.41434	136

F=70.3767.
P=0 at the 0.05 level.

CONCLUSIONS

Computational analysis of the urea ion channel of Helicobacter Pylori residing in our stomach gives the detail of its structure, disordered states and mutation sensitivity. It also predicts the ligand-binding site. The study reveals several disordered regions and mutation sensitivity in some residues. Missense mutations are observed for some residues. Further experimental studies along with the computational outcome may find the exact therapeutic target to treat the disease efficiently. The water-ion model of the channel protein shows the hydrophobic nature of MD simulation. The interaction of the protein with water and ions, and the water pathways inside the channel explain the interaction of the channel protein with our body environment. The failure in a clinical study of many potential nano drugs may be prevented by proper knowledge of the interaction of ion channels with body fluid and ions in the surroundings.

REFERENCES

[1] Muthu MS, Singh S. Targeted nanomedicines: Effective treatment modalities for cancer, AIDS and brain disorders. Nanomedicine 2009; 4(1): 105-118. https://doi.org/10.2217/17435889.4.1.105

[2] Deshpande PP, Biswas S, Torchilin V P. Current trends in the use of liposomes for tumor targeting. Nanomedicine, 2013; 8(9): 1509-28. https://doi.org/10.2217/nnm.13.118

[3] Bulbake U, Doppalapudi S, Kommineni N, Khan W. Liposomal Formulations in Clinical Use: An Updated Review. Pharmaceutics 2017; 9(4): 12. https://doi.org/10.3390/pharmaceutics9020012

[4] Lamichhane N, Udayakumar T, D'Souza W, Ii CS, Raghavan S, Polf J, Mahmood J. Liposomes: Clinical Applications and Potential for Image-Guided Drug Delivery. Molecules 2018; 23(2): 288. https://doi.org/10.3390/molecules23020288

[5] Mendes LP, Pan J, Torchilin V. Dendrimers as Nanocarriers for Nucleic Acid and Drug Delivery in Cancer Therapy. Molecules 2017; 22(9): 1401. https://doi.org/10.3390/molecules22091401

[6] Franiak-Pietryga I, Ziemba B, Messmer B, Skowronska-Krawczyk D. Dendrimers as Drug Nanocarriers: The Future of Gene Therapy and Targeted Therapies in Cancer. Dendrimers - Fundamentals and Applications 2018, InTech Open. https://doi.org/10.5772/intechopen.75774

[7] Li B, Li Q, Mo J, Dai H. Drug-Loaded Polymeric Nanoparticles for Cancer Stem Cell Targeting. Frontiers in Pharmacology 2017; 8: 51. https://doi.org/10.3389/fphar.2017.00051

[8] Ferrari R, Sponchioni M, Morbidelli M, Moscatelli D. Polymer nanoparticles for the intravenous delivery of anticancer drugs: The checkpoints on the road from the synthesis to clinical translation. Nanoscale 2018; 10(48): 22701-22719. https://doi.org/10.1039/C8NR05933K

[9] Wu M, Huang S. Magnetic nanoparticles in cancer diagnosis, drug delivery and treatment (Review). Molecular and Clinical Oncology 2017; 7(5): 738-746. https://doi.org/10.3892/mco.2017.1399

[10] Chang D, Lim M, Goos JA, Qiao R, Ng YY, Mansfeld, FM., . . . Kavallaris, M. Biologically Targeted Magnetic Hyperthermia: Potential and Limitations. Frontiers in Pharmacology 2018; 9: 831. https://doi.org/10.3389/fphar.2018.00831

[11] Son KH, Hong JH, Lee J W. Carbon nanotubes as cancer therapeutic carriers and mediators. International Journal of Nanomedicine 2016; 11: 5163-5185. https://doi.org/10.2147/IJN.S112660

[12] Sanginario A, Miccoli B, Demarchi D. Carbon Nanotubes as an Effective Opportunity for Cancer Diagnosis and Treatment. Biosensors 2017; 7(1): 9. https://doi.org/10.3390/bios7010009

[13] Frieboes H B, Wu M, Lowengrub J, Decuzzi P, Cristini V. A Computational Model for Predicting Nanoparticle Accumulation in Tumor Vasculature. PLOS ONE 2013; 8(2): e56876. https://doi.org/10.1371/journal.pone.0056876

[14] Cai Y, Wu J, Li Z, Long Q. Mathematical Modelling of a Brain Tumour Initiation and Early Development: A Coupled Model of Glioblastoma Growth, Pre-Existing Vessel Co-Option, Angiogenesis and Blood Perfusion. PLOS ONE 2016; 11: e0150296. https://doi.org/10.1371/journal.pone.0150296

[15] Brocato TA, Coker EN, Durfee P.N. *et al.* Understanding the Connection between Nanoparticle Uptake and Cancer Treatment Efficacy using Mathematical Modeling. Sci Rep 2018; 8: 7538. https://doi.org/10.1038/s41598-018-25878-8

[16] Dogra, P., Butner, J.D., Chuang, Yl. *et al.* Mathematical modeling in cancer nanomedicine: a review. Biomed Microdevices 2019; 21: 40. https://doi.org/10.1007/s10544-019-0380-2

[17] Sahai N, Gogoi M, Ahmad N. Mathematical Modeling and Simulations for Developing Nanoparticle-Based Cancer Drug Delivery Systems: A Review. Curr Pathobiol Rep 2021; 9: 1-8. https://doi.org/10.1007/s40139-020-00219-5

[18] Cheng YH, He C, Riviere J E, Monteiro-Riviere NA, Lin Z. Meta-Analysis of Nanoparticle Delivery to Tumors Using a Physiologically Based Pharmacokinetic Modeling and Simulation Approach. ACS Nano 2020; 14: 3075-3095. https://doi.org/10.1021/acsnano.9b08142

[19] Prevarskaya N, Skryma R, Shuba Y. Ion channels in cancer: Are cancer hallmarks oncochannelopathies? Physiol Rev 2018; 98(2): 559-621. https://doi.org/10.1152/physrev.00044.2016

[20] Leanza L, Managò A, Zoratti M, Gulbins E, Szabo I. Pharmacological targeting of ion channels for cancer therapy: In vivo evidences. Biochim Biophys Acta 2016; 1836(6 pt B): 1385-97. https://doi.org/10.1016/j.bbamcr.2015.11.032

[21] Bose T, Cieślar-Pobuda A, Wiechec E. Role of ion channels in regulating Ca^{2+} homeostasis during the interplay between immune and cancer cells. Cell Death Dis 2015; 6(2): e1648. https://doi.org/10.1038/cddis.2015.23

[22] Litan, A., Langhans, S.A. Cancer as a channelopathy: ion channels and pumps in tumor development and progression. Front. Cell. Neurosci 2015; 9: 86. https://doi.org/10.3389/fncel.2015.00086

[23] Lang F, Stournaras C. Ion channels in cancer: future perspectives and clinical potential. Philos Trans R Soc Lond B Biol Sci 2014; 369(1638): 20130108. https://doi.org/10.1098/rstb.2013.0108

[24] Storm P, Kjaer Klausen T, Trulsson M, Ho, JCS, Dosnon M *et al.* A Unifying Mechanism for Cancer Cell Death through Ion Channel Activation by HAMLET. PLOS ONE 2013; 8(3): e58578. https://doi.org/10.1371/journal.pone.0058578

[25] Șterbuleac D, Maniu CL. An antiarrhythmic agent as a promising lead compound for targeting the hEAG1 ion channel in cancer therapy: insights from molecular dynamics simulations. Chem Biol Drug Des 2016; 88(5): 683-689. https://doi.org/10.1111/cbdd.12797

[26] Cervera J, Alcaraz A, Mafe S. Bioelectrical Signals and Ion Channels in the Modeling of Multicellular Patterns and Cancer Biophysics. Sci Rep 2016; 6: 20403. https://doi.org/10.1038/srep20403

[27] Kelley L, Mezuli S, Yate C. *et al*. The Phyre2 web portal for protein modeling, prediction and analysis. Nat Protoc 2015; 10: 845-858. https://doi.org/10.1038/nprot.2015.053

[28] Wass MN, Kelley LA, Sternberg MJ. 3DLigandSite: predicting ligand-binding sites using similar structures. Nucleic Acids Res 2010; 38(Web Server issue): W469-W473. https://doi.org/10.1093/nar/gkq406

[29] Oberholser K, Sussman J L, Hodis E, Decatur W, Livne S, Prilusky J, Richardson JS, Berchansky A. 2013, "Ramachandran Plot", Proteopedia, https://doi.org/10.14576/381225.1772128

[30] Le Guilloux V, Schmidtke P, Tuffery P. Fpocket: An open source platform for ligand pocket detection. BMC Bioinformatics 2009; 10: 168. https://doi.org/10.1186/1471-2105-10-168

[31] Yates CM, Filippis I, Kelley LA, Sternberg MJ. SuSPect: enhanced prediction of single amino acid variant (SAV) phenotype using network features. J Mol Biol 2014; 426(14): 2692-701. https://doi.org/10.1016/j.jmb.2014.04.026

[32] McNulty R, Ulmschneider J, Luecke H. *et al.* Mechanisms of molecular transport through the urea channel of Helicobacter pylori. Nat Commun 2013; 4: 2900. https://doi.org/10.1038/ncomms3900

[33] Strugatsky D, McNulty R, Munson K. *et al.* Structure of the proton-gated urea channel from the gastric pathogen Helicobacter pylori. Nature 2013; 493: 255-258. https://doi.org/10.1038/nature11684

[34] Suzuki R, Satou K, Shiroma A, Shimoji M, Teruya K, Matsumoto T, Akada J, Hirano T, Yamaoka Y. Genome-wide mutation analysis of Helicobacter pylori after inoculation to Mongolian gerbils. Gut pathogens 2019; 11: 45. https://doi.org/10.1186/s13099-019-0326-5

[35] Breed J, Sankararamakrishnan R, Kerr I D, Sansom MS. Molecular dynamics simulations of water within models of ion channels. Biophysical journal 1996; 70(4): 1643-1661. https://doi.org/10.1016/S0006-3495(96)79727-8

[36] Copie G, Cleri F, Blossey R. *et al.* On the ability of molecular dynamics simulation and continuum electrostatics to treat interfacial water molecules in protein-protein complexes. Sci Rep 2016; 6: 38259. https://doi.org/10.1038/srep38259